Title	Automatic Recognition of Weld Defects in Radiographic Test (Report 1) : Extraction of Feature Parameters(Welding Mechanics, Strength & Design)
Author(s)	Inoue, Katsunori; Kobayashi, Masafumi
Citation	Transactions of JWRI. 1982, 11(2), p. 123-132
Version Type	VoR
URL	https://doi.org/10.18910/12280
rights	
Note	

Automatic Recognition of Weld Defects in Radiographic Test (Report 1)[†]

— Extraction of Feature Parameters —

Katsunori INOUE[*] and Masafumi KOBAYASHI[**]

Abstract

The digital image processing was applied to automatic recognition of weld defects in a radiographic test. The radiographic image was converted into digital data which were further processed to extract the image of weld defect from the processed data and sort out the defect by the type of defect according to algorithmic procedure.

KEY WORDS: (Nondestructive Testing) (Radiography) (Digital Processing) (Automatic Recognition) (Image Processing)

1. Introduction

A radiographic test is commonly used as the nondestructive inspection of a weld joint.

In this inspection, evaluation and judgement of radiographic findings are achieved by human eyes at present. Needless to say, however, human judgement involves a difficulty or rather impossibillity in maintaining consistent immutability of inspection standards and in avoiding shortcomings arising from the subjective differences among individual inspectors and the changes of passing time.[1] Introduction of a processing system replaced by machine has been studied[2)–5)] to solve this problem and to meet the need of labor-saving.

The machine processing system may be composed of several stages. In the first stage, image processing is introduced as a subsidiary means to make human judgement easier, for instance, by emphasizing the defect image or removing the change in brightness of weld reinforcement. In the second stage, processing is performed in the form of man-to-machine conversation, in which machine-aided works such as measurement of the area and length, quantitative determination of the index of configuration and calculation of the number of particles and massive grains in the area indicated by the inspector are accomplished. In the third stage, almost all processings including automatic detection and rejection of conspicuous defects are achieved by machine. Human judgement participates only in whatever defects a machine is unable to process. This stage may eventually be further improved into the final stage. In the final stage, the machine system can pick up all the images of weld defects, count their numbers, sort out the defects according to their size and shape and make judgement of the results, fully automatically throughout the entire course of inspection.

Although application of a digital image processing[6),7)] is required for performing such processing operations, the present image processing technique does not yet allow processing of the third and the final stages. because of its various problem. Inspection by this technique in these stages, therefore, has not as yet come into common use.

This paper describes the pursuit of the possibility of realization of fully automatic inspection in the above mentioned third and final stages by analyzing the characteristics of radiographic findings of weld joints and the image features of weld defects.

2. Outline of Processing Apparatus and Processing System

2.1 Processing apparatus

The processing apparatus is composed of an image pickup device and an arithmetic operation device. **Figure 1** shows a block diagram of the image pickup device. The video signal from a TV camera (Hamamatsu TV Co., Ltd. C1000) is converted into a digital value of 8 bit under control of CPU (Microprocessor, Intel 8080A). Sampling of data from an arbitrary position in the picture frame is possible by setting the value of the comparator, because X and Y address signals which correspond to the position of the video signal are delivered from the camera controller. This hardware permits sampling of 1,024 (horizontal) x 1,024 (vertical) = 1,048,576 points at the maximum in
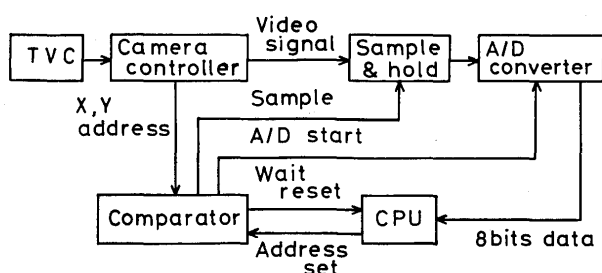
Fig. 1 Block diagram of image pickup device.
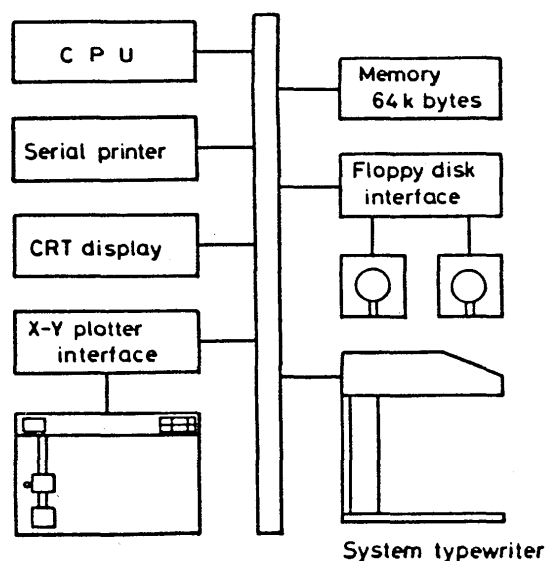
Fig. 2 Block diagram of arithmetic operation device.

Fig. 3 Schema of processing software.

a frame of picture. **Figure 2** shows a block diagram of the arithmetic operation device having CPU used in common with the image pickup device. The pre-and post-process image data can be displayed on CRT which is an intelligence terminal having CPU and buffer momeory of 12 K bytes with pixels of 256 x 256 points.

2.2 Processing system

A schematic diagram of the software processing system which is implemented on the above described hardware is shown in **Fig. 3**. The system is divided into two parts, a learning system and an automatic sorting system.

In the learning system, processing is carried out by the following steps on the basis of films recorded with pre-classified defects (classified by visual observation of licensed persons).

a. Digital conversion of an image and input into the arithmetic opration system.

b. Extraction of defect images from the back-ground and discrimination of these images individually.

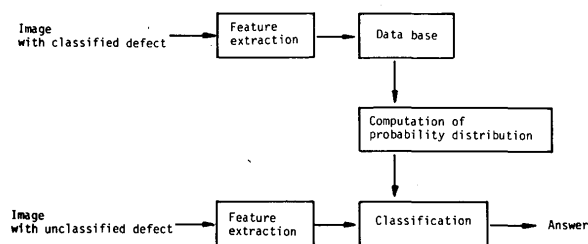c. Calculation of the parameters of defect feature from the shape and size of the defect image.

d. Plotting of the obtained values of the parameters in the feature space.

e. Calculation of the probability density of any particular defect distributed in the feature space.

f. Calculation of the distribution of the probability density of various defects appearing in the feature space.

In stages e and f, the reliability of the calculation results increases by repetition of data input, because of accumulation of the processed results of the input data.

In the automatic sorting system, the image of defect in an unclassified film is fed and the type of the defect is estimated. In this system, after going through the same steps $a \sim c$ as applied to the learning system, the data are processed by the below mentioned steps.

d. Mapping the point of defect in the feature space from the calculated value of feature.

e. Estimating the probability of the occurrence of a specific defect from the a posteriori probability of various defects on that point in the feature space.

Operations in these steps are detailed in the following chapter.

3. Image of Weld Defect and Method of Its Extraction

3.1 Radiographic characteristics of weld joint

Weld joints are usually mounted with reinforcement which is in most cases left without shaping or grinding. Therefore, radiographically the exposure to radiation decreases in the region of reinforcement, resulting in increased brightness on the film, as shown in **Fig. 4(a)**. The horizontal distribution of brightness in the region indicated by an arrow in the firgure (which contains defects) appears as shown in **Fig. 4(b)**. The change in the brightness due to the defect is thus sharper than that caused by reinforcement. Namely, it has components of high frequency and at the same time a larger absolute value of change, as compared with the components of high frequency noise. This phenomenon can be utilized for extraction
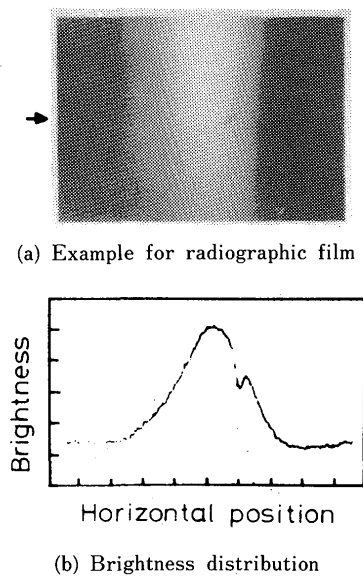
(a) Example for radiographic film

(b) Brightness distribution

Fig. 4 Example for radiographic film of weld joint with a defect and its brightness distribution.

(a) Blowhole (c) Lack of fusion
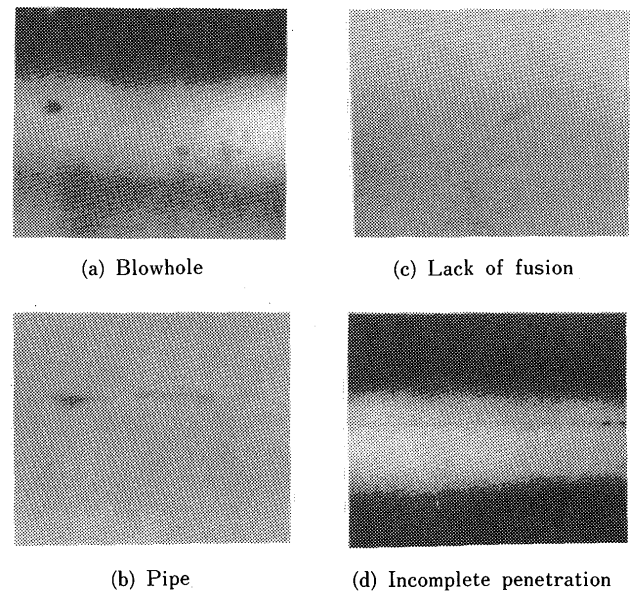
(b) Pipe (d) Incomplete penetration

Fig. 5 Photographes of typical weld defects.

of defect from the reinforcement region.

3.2 Image of weld defect

The inner defects in a weld joint that appear in radiographic films can be divided as under.
a. Blowhole
b. Pipe
c. Slag inclusion
d. Lack of fusion
e. Incomplete penetration
f. Cracking

Of these, f is very frequently regarded as one of the most malignant types of weld defects. However, as it is effectively detected by other more sensitive inspection method such as an ultrasonic test, a - e, excluding f, are taken up in this study. **Figure 5** shows the photographes of these types of defct.

3.3 Extraction process of defects

3.3.1 Outline

The extraction process of defects is performed by the following steps.
a. Sampling of an image and digital conversion.
b. Elimination of back-ground noise.
c. Detection of a boundary line between the base metal and weld part.
d. Extraction of brightness change due to reinforcement.
e. Extraction of a defect.
f. Smoothing operation.
g. Tracking of the outlines of defects and recognition
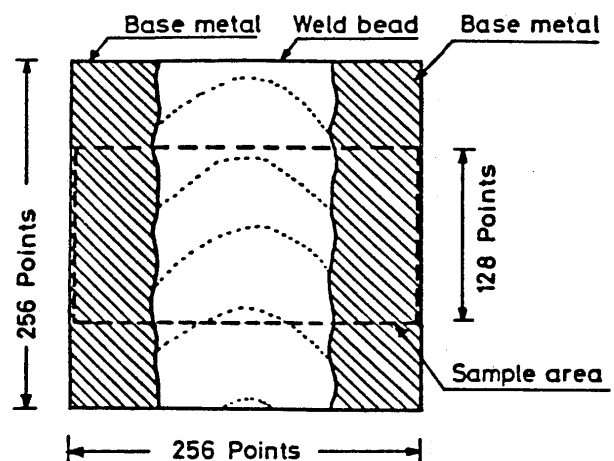

Fig. 6 Illustration of sampled area.

of an individual defect.

These steps are explained in the following.

3.3.2 Sampling of an image and digital conversion

The object is photographed with a TV camera, fixing the visual field so that the boundary lines between the base metal and weld part fit vertically in the position a quarter distant from both the left and right sides of the screen (see **Fig. 6**). The total of 32,768 points, 256 horizontally and 128 vertically, are sampled from this screen and converted into digital by 8 bit. The converted image data are saved into memory.

3.3.3 Elimination of back-ground noise

The digital image data obtained contain high fre-

quency noise. The noise components are, therefore, eliminated by smoothening 3 consecutive data through the running mean for every horizontal scanning line using Eq. (1).

$$D_1(i, j) = \frac{1}{3} \sum_{p=-1}^{1} D(i + p, j) \qquad (1)$$

where $D(i, j)$ represents the brightness of (i, j) point ($i = 1 \cdots\cdots 256$, $j = 1 \cdots\cdots 128$) and $D_1(i, j)$ is the smoothened value. The brightness distribution for the same horizontal scanning line before and after noise elimination is shown in **Fig.7 (a)** and **(b)** respectively.
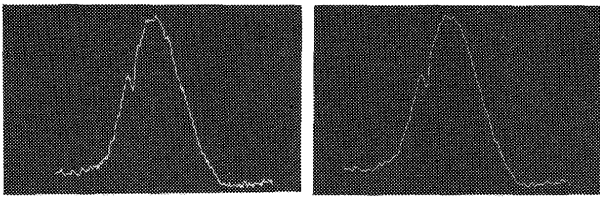
(a) Before smoothing operation (b) After smoothing operation

Fig. 7 Brightness distribution on a horizontal scanning line of weld •part.

3.3.4 Detection of a boundary line between the base metal and weld part

Since defects occur only in a weld joint, the area of defect detection has to be restricted to the region of the weld joint by detecting the boundary line between the base metal and weld part.

The data of the weld joint in the center of the screen and the data of the base metal on the left and right sides of the screen for every horizontal scanning line are approximated by the curve of second degree and the straight line respectively, from which the intersections are obtained. The boundary line is determined from the linked intersections. In this approximate calculation, choosing 20 points at every 4 points in the center of the screen for the weld joint and 10 points at every 4 points both from the left and right ends of the screen for the base metal, the curve of second degree and straght line are calculated by the method of least squares on the basis of these points as the data.
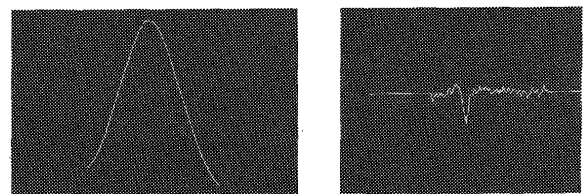
3.3.5 Extraction of brightness change due to reinforcement

The net change in the brightness caused only by the defect can be determined by subtracting the brightness change due to reinforcement from the total brightness change in the horizontal (vertical to the weld line) direction. In order to extract the change in the low frequency brightness that corresponds to the brightness change due to reinforcement, the data of

this region are approximated by the curve of second degree. Operation of convolution by the method of least squares[8] was performed for this calculation using the following Eq. (2).

$$D_2(i, j) = \frac{1}{CK} \sum_{p=-n}^{n} D_1(i + p, j) C(p) \qquad (2)$$

where CK and $C(p)$ are predetermined constants and $D_1(i, j)$ is provided by Eq. (1). In this calculation, n is put as 8. $D_2(i, j)$ is the approximated value. $D_2(i, j)$ and $\Delta D(i, j)$ ($= D_1(i, j) - D_2(i, j)$) obtained by applying Eq. (2) to the data of $D_1(i, j)$ in Fig. 6(b) are shown in **Fig. 8(a)** and **(b)** respectively.
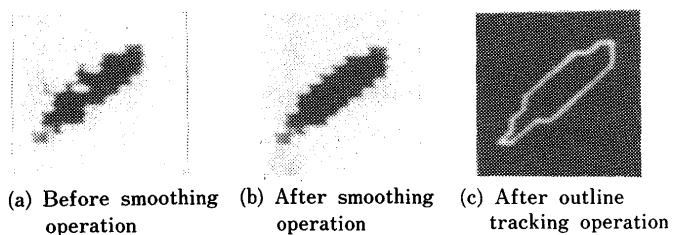

(a) Extraction of brightness change (b) Result of extraction of
    due to weld reinforcement   weld defect

Fig. 8 Results of extraction procedure.

$\Delta D(i, j)$ is converted into binary by the threshold D_{th} obtained from the photographic density of contrast meter.

$$D_3(i, j) = \begin{cases} 1 \cdots\cdots \Delta D(i, j) \leq D_{th} \\ 0 \cdots\cdots \Delta D(i, j) > D_{th} \end{cases} \qquad (3)$$

$D_3(i, j)$ is now the binary image data in which the background is 0 and the defect is 1, as shown in **Fig. 9(a)**.

(a) Before smoothing   (b) After smoothing   (c) After outline
    operation   operation   tracking operation

Fig. 9 Binary image of a defect.

3.3.6 Smoothing operation

As shown in Fig. 9(a), the binary image includes noise and shows the boundary line of conspicuous irregularity. As such irregularity causes inconvenience for subsequent processes, smoothing operation is performed by examining the continuity of binary data and rectifying so that the isolated point does not exist in the binary data. The flowchart for the smoothing operation is shown in **Fig. 10**. In this operation, the value of 0 or 1 which is major in the odd numbers of the data including the present checking point and the
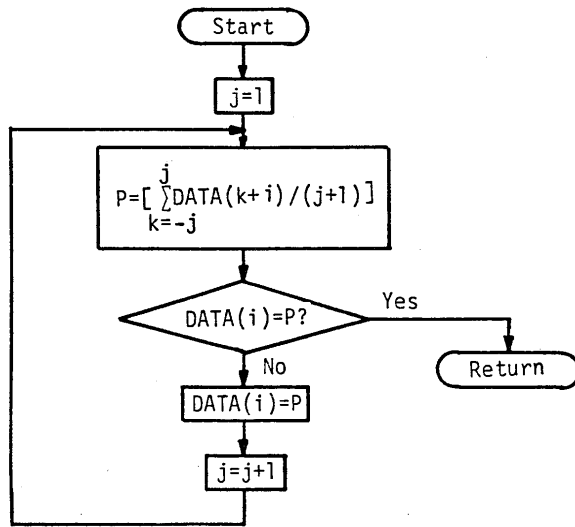
Fig. 10 Flowchart for smoothing algorithm.

points in its neighborhood is set as the valne of the checking point. This process was carried out by searching the data horizontally first and vertically then. The smoothed image is shown in **Fig.9(b)**. The figure is transformed into a more smooth image, as compareed with Fig. 9(a).

3.3.7 Tracking of the outlines of defects and recognition of an individual defect

Individual discrimination of each defect converted into binary data is required for obtaining information of each defect. A group of points with continuity of 1 is defined as a defect. To achieve this, the binary image data are firstly searched to find the one point which exists on the outline of the defect. Using this point as a starting point, adjacent point that form the defect outline are searched in accordance with a certain rule. The points of outline are tracked one after another by repeating the above procedure until all points are

Fig. 11 Flowchart for outline tracking operation.

connected to the starting point. On completion, the area enclosed by these points is marked as a defect. The flowchart of algorithm for tracking the outline is shown in **Fig. 11**. **Figure 9(c)** is an example of outline of the defect shown in Fig. 9(b), extracted by this process.

4. Features of Defect and Their Parameters Calculation

4.1 Features of defect[9],[10]

Radiographical features of defects which whre shown described as under.

4.4.1 Blowhole

A blowhole is a bubble formation within the deposited metal mostly in the form of a spherical cavity. It appears on a film as a relatively well-defined round or elliptical image. It can be distinguished by the feature amount contained in the shape.

4.1.2 Pipe

A pipe is a thin and narrow extension of bubbles along the crystal growth. This can be distinguished from a blowhole by the presence of a constricted and elongated portion.

4.1.3 Slag inclusion and lack of fusion

A slag inclusion is caused as a result of remaining flux within the deposited metal. A lack of fusion is a state of insufficient fusion between the deposited metal and base metal or between the deposited metal. As compareed with a blowhole or pipe, they usually assume a crushed configuration, frequently with an indistinct borderline. The shape is of distorted irregularity.

4.1.4 Incomplete penetration

Incomplate penetration is a state in which the root remains completely unfused. This appears on a film as a thin line, usually in parallel with a bead.

4.2 Calculation of feature parameters

The following feature parameters were defined on the basis of various features of each defect so that the defects can be discriminatively classified.

4.2.1 Flatness

In order to discriminate very thin defects like incomplete penetration from other defects, the image flatness was quantitatively determined. The flatness was defined as the dimensionless value $FLT = I_p/S^2$
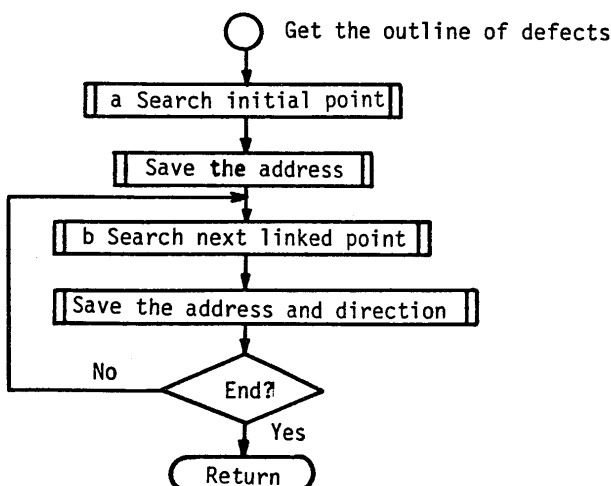
obtained by dividing the polar moment of second order I_p around the center of defect image by the square of its area S^2. In the ellipse with the ratio of major/minor axis $= 1 : p$, this value is $(p+1/p)/4\pi$.

4.2.2 Symmetry

Although a blowhole image can be regarded as almost elliptical, a pipe is shaped with one end constricted and elongated as previously described. These defects are distinguished by the symmetry in the direction of major axis. As shown in **Fig. 12**, therefore, after obtaining the major axis, the areas S_1 and S_2 (shadowed portions) on the both sides divided by 2 perpendicular lines that pass internally across the major axis separating the defect into 3:1 and 1:3. When $P_1 > S_2$, the degress of symmetry is defined as $SYM = S_2/S_1$. Needless to say, $0 < SYM \leqq 1$. The typical examples of a pipe on the upper side and a blowhole on the lower are shown in Fig. 12. SYM is larger in the lower figure.
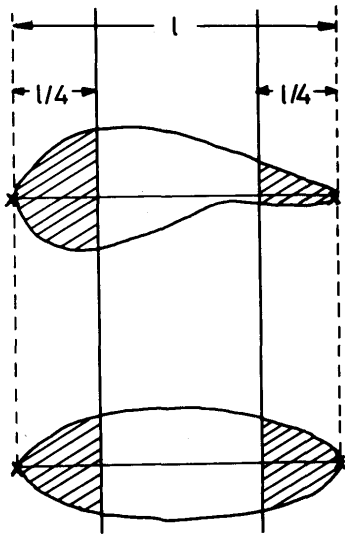

Fig. 12 Difinition for the index of symmetry.

4.2.3 Unsharpness

The unsharpness is defined as the ratio of the sum of S_1 and S_2 obtained as above to the entire area S, i.e., $USP = (S_1 + S_2)/S$. USP is 0.39 for an elliptical shape and 0.25 for a rhombic shape.

4.2.4 Direction of major axis

In order to discriminate the defects that run parallel with the weld line like incomplete penetration, the supplementary angle θ formed by the major axis and weld line is defined as the major axial direction as shown in **Fig. 13**. θ is calculated by the following equation.
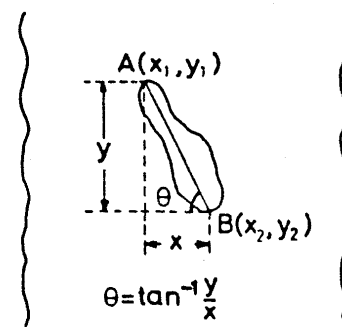

Fig. 13 Difinition for the index of direction of major axis.

$$\theta = \tan^{-1}\frac{Y_1 - Y_2}{X_1 - X_2} \qquad (4)$$

4.2.5 Position

The value obtained by dividing the distance a_1 between the center of defect figure and the weld line (the center line of weld) by the weld width B_w is defined as the position $PG = (a_1/B_w)$ as shown in **Fig. 14**.
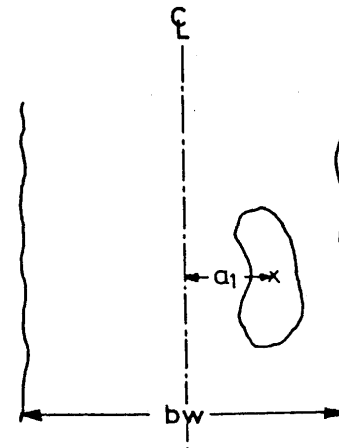

Fig. 14 Difinition for the index of position.

5. Measurement of the Incidence of Feature Parameters

5.1 Outline

The incidence of each defect was determined by calculating the the feature parameters (ref: Chapter 4) from the weld defect extracted by the method shown in Chapter 3 from several hundreds of radiographic films of weld joints which are recorded with categorized defects (classified by a licensed inspector). On the basis of the results obtained, appropriate parameters and their combinations for estimating the specific defect were examined.

5.2 Flatness

The distribution of frequency of flatness for each

type of defect is shown together in **Fig. 15**, in which the flatness is plotted on a horizontal axis and the frequency on a vertical axis. This value increases for a thin and long defect, as defined in the preceding chapter. As predicted, incomplete penetration, as compared with other types of defect, is distriubted in the region of large value. This allows discrimination of incomplete penetration from other defects.
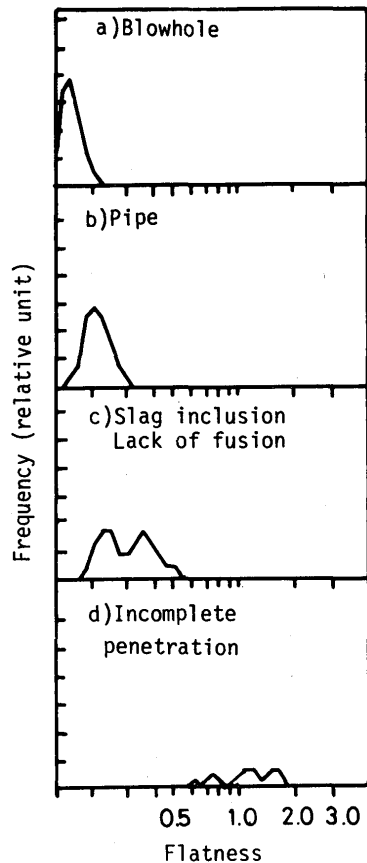

Fig. 15 Frequency distribution of flatness for each defect.

5.3 Symmetry

The frequency distribution of the symmetry for each defect was likewise obtained and shown in **Fig. 16**. The value decreases with the loss of symmetry. As already described, this can be used for distinguishing a blowhole and pipe (see a) and b) of this figure).

5.4 Unsharpness

The frequency distribution of Unsharpness for each defect is shown in **Fig. 17**. Although slag inclusion and lack of fusion show a more broader distribution than other defects, this is not a determinative factor for discrimination. Combining the factor of symmetry together, **Fig. 18(a)** is obtained by two-dimensional arrangement. When the plane based on the 2 para-
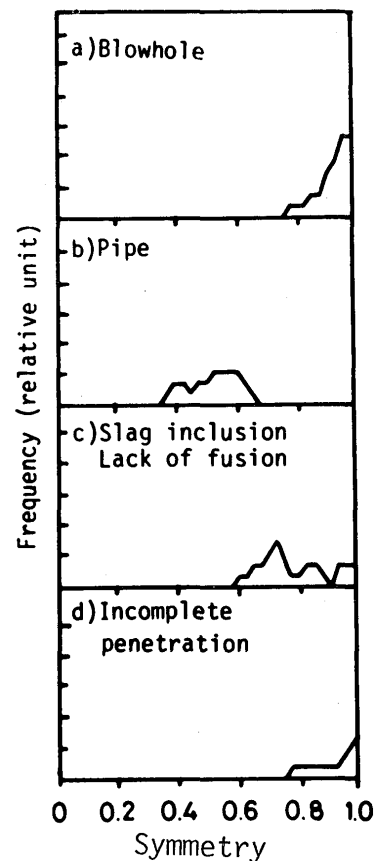

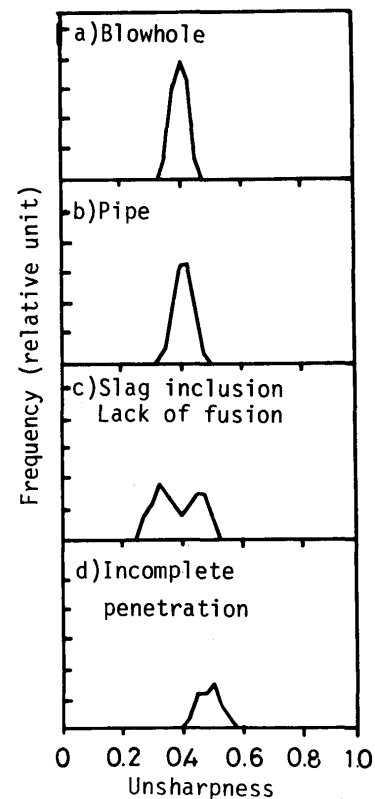**Fig. 16** Frequency distribution of symmetry for each defect.

Fig. 17 Frequency distribution of unsharpness for each defect.
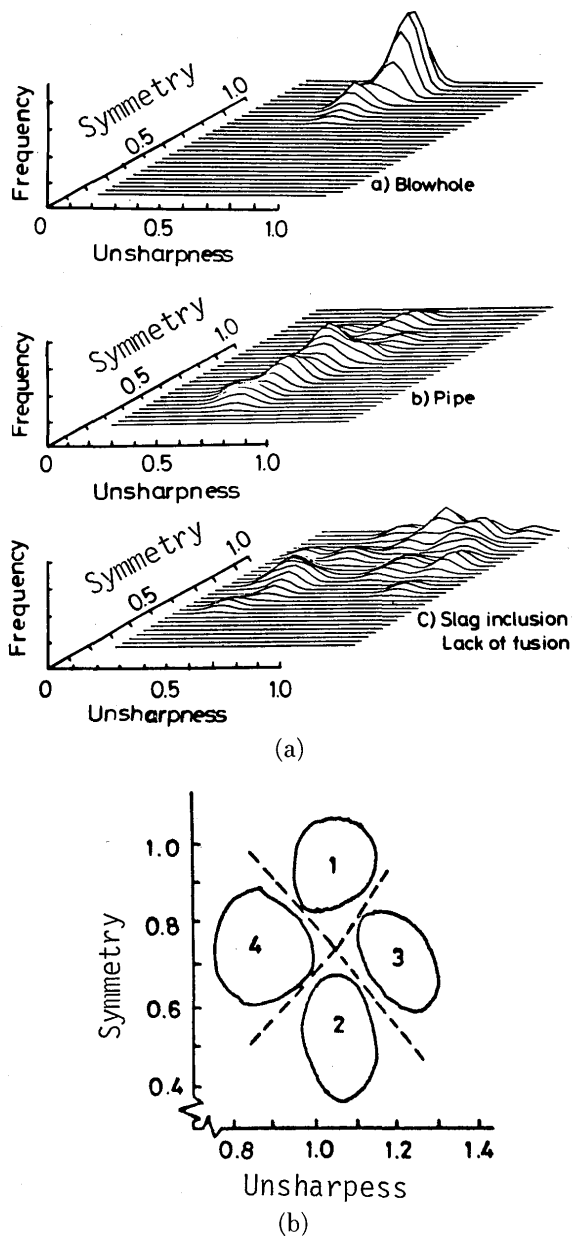
(a)

(b)

Fig. 18 Two-dimensional frequency distribution of symmetry-unsharpess plane for each defect.

meters is divided into 4 regions as shown in **Fig. 18(b)**, it is noted from (a) that the regions 1 and 2 correspond to a blowhole and pipe. The regions 3 and 4 correspond to a slag inclusion and lack of fusion and are characterized by irregularity of shape.

5.5 Others

Figure 19 (a) and (b) show the frequency distribution of major axial direction and position. No noteworthy findings are observed on the whole with the exception of the appearance (though naturally) of incomplete penetration in the center of the bead along the weld line.
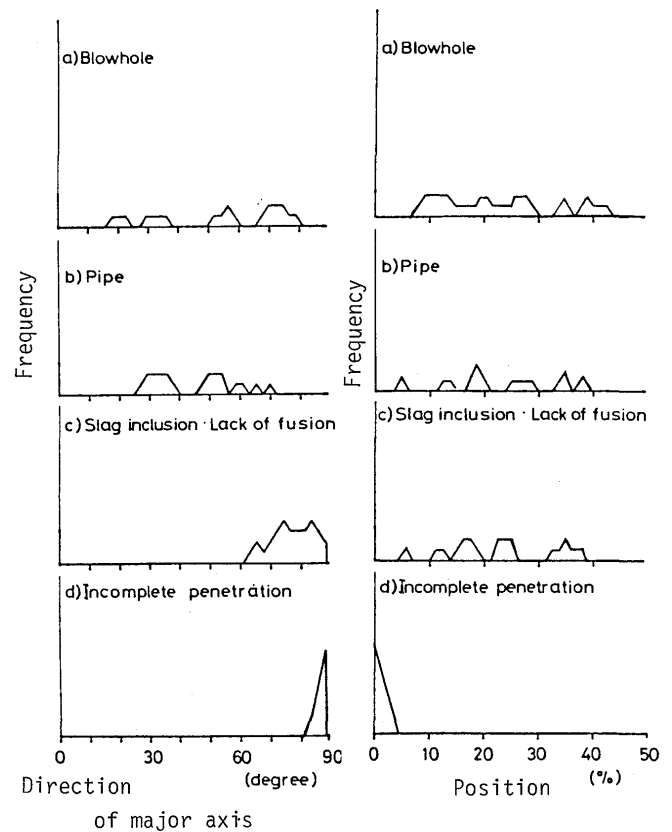

Fig. 19 Frequency distribution of other parameters.

6. Distribution of A Posteriori Probability and Automatic Sorting of Defects

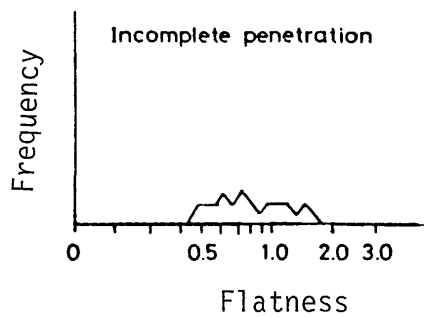### 6.1 Calculation of a posteriori probability distribution

The a posteriori probability P(X) of each defect for parameter X was calculated from the frequency distribution of various parameters of each defect by Eq. (5) (Bayes rule[11]).

$$P_i(X_K) = \frac{A_i(Xk)}{\sum_{j=1}^{N} A_j(Xk)} \qquad (i = 1 \cdots\cdots N) \quad (5)$$

where $A_i(X_k)$ is the incidence of defect i corresponding to feature parameter X_k and N is determined to be 4 in accordance with the number of defect types in this study.

6.2 Distribution of a posteriori probability for incomplete penetration

Figure 20 (a) and (b) show the histogram of incomplete penetration (same as Fig. 15(d)) and histogram of other defects in terms of flatness. These data provide the occurrence probability (a posteriori probability: vertical axis) of incomplete penetration in terms of a feature parameter, flatness (horizontal axis) by Eq. (5) as shown in **Fig. 21**.

Incomplete penetration

(a) For incomplete penetration
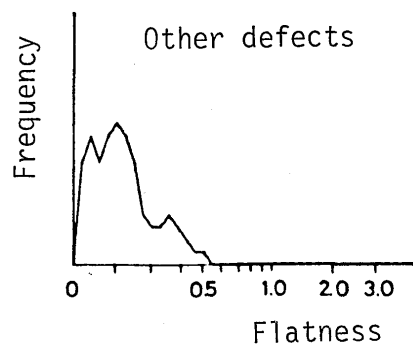
Other defects

(b) For other defects

Fig. 20 Frequency distribution of flatness for incomplete penetration and other defects.
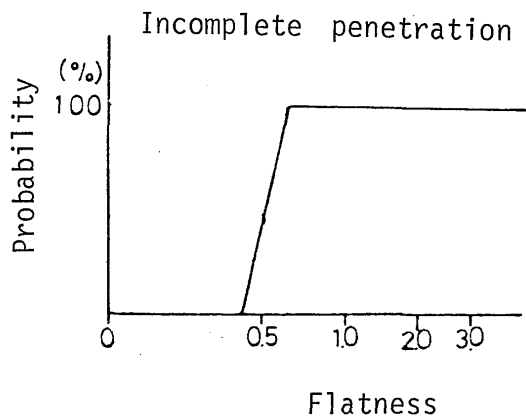
Incomplete penetration

Fig. 21 A posteriori probability of incomplete penetration.

a)Blow hole

b)Pipe

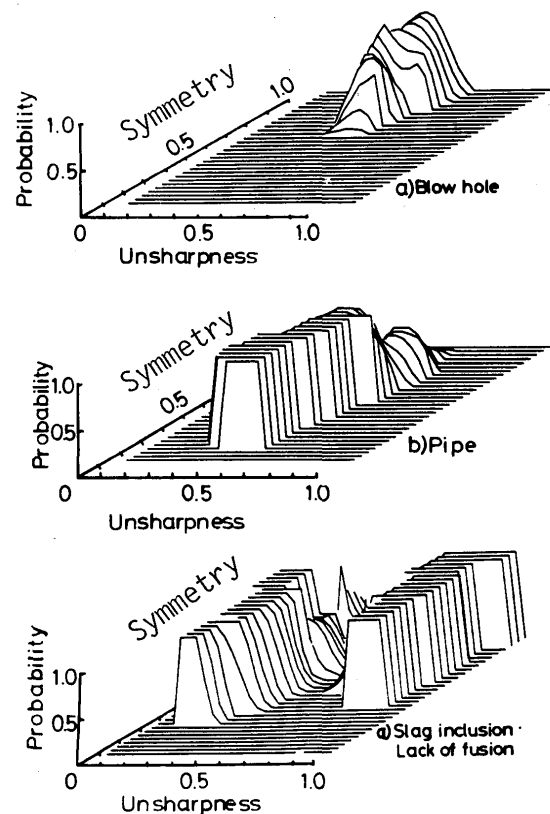a)Slag inclusion Lack of fusion

Fig. 22 A posteriori probabillity of blowhole, pipe, slag inclusion and lack of penetration.

6.4 Automatic sorting

The algorithm that permits discrimination of an unidentified defect on the basis of the results obtained in 6—2 and 6—3 is as under.

Three feature parameters, i.e., flatness, sharpness and symmetry, are firstly analyzed from the defect image extracted from the film. The defect is then discriminated from Fig. 21, whether incomplete penetration or other types of defect. If the defect was the latter, the type of the defect, whether a blowhole, pipe, slag inclusion or lack of fusion, is further judged from Fig. 22. In case of a failure in judgement of the type of defect in spite of this double collation, it is also indicated as an output datum.

As described above, since judgement is strictly based on the a posteriori probability distribution of feature parameters, highly reliable definition of feature parameters is a prerequisite for avoidance of misjudgement. Input of adequate data is, therefore, required in the learning system.

6.3 Distribution of a posteriori probability for blowhole, pipe, slag inclusion and lack of fusion

Likewise, the a posteriori probability (W axis) of blowhole, pipe, slag inclusion and lack of fusion in terms of feature parameters, sharpness (Y axis) and symmetry (Z axis) can be obtained as shown in **Fig. 22** from the two dimensional distribution of each defect shown in Fig. 18(a).

7. Summary

This paper is summarized as under.
1) The method of extracting the defect image from the

radiographic films of weld joint by application of a digital image processing technique was described.

2) It was found that various types of defects could be discriminated from the feature parameters of extracted defect image.

3) The possibility of automatic sorting of weld defects by the combined organization of learning and automatic sorting systems on the basis of algorithm introduced in 1) and 2) was shown.

The problems in and the future course of this study may include the following.

1) Extraction of a larger amount of feature parameters from a multi-gradiation image, instead of a binary image, in image processing may contribute to more effective utilization of defect information from an image. The dynamic range for digital conversion may have to be increased to larger capacity (12 or 16 bit) from 8 bit.

2) The learning system should be organized by more advanced theory for calculation of a posteriori probability or the decision making from the calculated value.

References

1) The Japanese Society for Non-Destructive Inspection: "Hoshasen Toka Shashin no Tokyu Bunrui", (1978) (in Japanese)

2) Y.Shirai: "Automatic Inspection of X-ray Photograph of Welding", Pattern Recognition, Vol.1 (1969), p.257—261

3) M.Takagi and Y.Yokoi: "Yosetsubu X-senzo no Digital Shori", J. of NDI, Vol.22, No.9. (in Japanese)

4) T.Fujita, Y.Hioki and H.Matsui: "Processing of Radiographic Images of Non-Destructive Weld Testing", The Hitachi Zosen Technical Review, Vol. 39 (1978),No.4, p.1—6. (in Japanese)

5) H.Koshimizu and T.Yoshida: Trans. of IECE, 10 (1981), p.983.

6) A.Rosenfeld: "Picture Processing by Computer", Academic Press.

7) M.Nagao: "Future Extraction and Recognition of Pictures", J. of IECE of Japan, Vol.59, p.1181—1186. (in Japanese)

8) A.Savitzky and M.J.E.Golay: "Smoothing and Differentiation of Data by Simplified Least Squares Procedures", Ana. Chem, Vol.36 (1964), No. 8, p.1627—1638.

9) The Japanese Society Non-Destructive Inspection: "Hihakai Shiken no Kiso to Yogo", Japan Management Association.

10) The Japanese Society for Non-Destructive Inspection: "Yosetsubu no Hoshasen Toka Shashin Gijutsu nikansuru Shashinshu ".

11) R.O.Duda and P.E.Hart: "Pattern Classification and Scene Analysis" p.11 John Wiley & Sons.